Journal of Controlled Release 233 (2016) 29–38

Contents lists available at ScienceDirect

Journal of Controlled Release

journal homepage: www.elsevier.com/locate/jconrel

cRGD-functionalized reduction-sensitive shell-sheddable biodegradable micelles mediate enhanced doxorubicin delivery to human glioma xenografts *in vivo*

Yaqin Zhu [a,b], Jian Zhang [a,*], Fenghua Meng [a], Chao Deng [a], Ru Cheng [a], Jan Feijen [a,b,**], Zhiyuan Zhong [a,*]

[a] Biomedical Polymers Laboratory, and Jiangsu Key Laboratory of Advanced Functional Polymer Design and Application, College of Chemistry, Chemical Engineering and Materials Science, Soochow University, Suzhou 215123, PR China

[b] Department of Polymer Chemistry and Biomaterials, Faculty of Science and Technology, MIRA Institute for Biomedical Technology and Technical Medicine, University of Twente, P.O. Box 217, 7500, AE, Enschede, The Netherlands

ARTICLE INFO

Article history:
Received 22 December 2015
Received in revised form 28 April 2016
Accepted 6 May 2016
Available online 10 May 2016

Keywords:
cRGD
Reduction-sensitive
Shell-sheddable
Biodegradable micelles
Doxorubicin
Targeted delivery

ABSTRACT

Biodegradable micelles are one of the most studied systems for the delivery of hydrophobic anticancer drugs. Their therapeutic efficacy *in vivo* is, however, suboptimal, partly due to poor tumor cell uptake as well as slow intracellular drug release. Here, we show that cRGD-functionalized intracellularly shell-sheddable biodegradable PEG-SS-PCL micelles mediate enhanced doxorubicin (DOX) delivery to U87MG glioma xenografts *in vivo*, resulting in significantly improved tumor growth inhibition as compared to reduction-insensitive cRGD/PEG-PCL controls. cRGD/PEG-SS-PCL micelles revealed a small size of *ca.* 61 nm, a decent DOX loading of 14.9 wt%, and triggered drug release in a reductive environment (10 mM glutathione). Flow cytometry, confocal microscopy, and MTT assays demonstrated that cRGD/PEG-SS-PCL micelles with a cRGD ligand density of 20% efficiently delivered and released DOX into $\alpha_v\beta_3$ integrin overexpressing U87MG cells. The *in vivo* pharmacokinetics studies displayed that DOX-loaded cRGD20/PEG-SS-PCL micelles had a prolonged elimination half-life time of 3.51 h, which was comparable to that of cRGD20/PEG-PCL counterparts, indicating that disulfide bonds in the PEG-SS-PCL micelles are stable in the circulation. Notably, *in vivo* imaging and biodistribution studies in U87MG glioma xenografts showed that cRGD20/PEG-SS-PCL micelles led to efficient accumulation as well as fast drug release in the tumor. The therapeutic outcomes demonstrated that DOX-loaded cRGD20/PEG-SS-PCL micelles exhibited little side effects and superior tumor growth inhibition as compared to non-targeting PEG-SS-PCL and reduction-insensitive cRGD20/PEG-PCL counterparts. The reduction-sensitive shell-sheddable biodegradable micelles have appeared as a fascinating platform for targeted tumor chemotherapy.

1. Introduction

Biodegradable micelles based on poly(ethylene glycol)-poly(ε-caprolactone) (PEG-PCL), poly(ethylene glycol)-polylactide (PEG-PLA), and poly(ethylene glycol)-poly(lactide-*co*-glycolide) (PEG-PLGA) block copolymers are among the most important nanosystems for anticancer drug delivery [1–3]. These micelles offer several unique advantages such as excellent biocompatibility, *in vivo* biodegradability, and approval for human use by the US Food and Drug Administration (FDA) [4,5]. A couple of biodegradable polymeric nanotherapeutics, *e.g.* Genexol-PM (micellar paclitaxel) and BIND-014 (docetaxel nanoparticulates), have advanced to the clinic or clinical trials [6–8]. It should be noted, however, that these micellar drugs exhibit suboptimal therapeutic efficacy *in vivo*, partly due to poor tumor cell uptake as well as slow intracellular drug release (as a result of gradual polymer degradation) [9–11].

Interestingly, we and Wang et al. found independently that incorporation of a disulfide bond between hydrophilic and hydrophobic blocks could significantly enhance the intracellular drug release and *in vitro* antitumor efficacy of biodegradable micellar drugs [12–14]. These reduction-sensitive shell-sheddable biodegradable micelles exhibit similar physicochemical and colloidal properties to the traditional ones (reduction-insensitive counterparts) as polymer modification is minimal. In recent years, several groups reported that reduction-sensitive shell-sheddable micelles based on amphiphilic block copolymers with different architectures and structures have all shown a triggered drug release behavior and markedly improved antitumor activity in various tumor cells as compared to their reduction-insensitive counterparts [15–28]. Galactose-decorated PEG-SS-PCL micelles were shown to efficiently deliver and release doxorubicin (DOX) into the nuclei of HepG2

* Corresponding authors.
** Correspondence to: J. Feijen, Department of Polymer Chemistry and Biomaterials, Faculty of Science and Technology, MIRA Institute for Biomedical Technology and Technical Medicine, University of Twente, P.O. Box 217, 7500, AE, Enschede, The Netherlands.
E-mail addresses: jianzhangsd@suda.edu.cn (J. Zhang), j.feijen@tnw.utwente.nl (J. Feijen), zyzhong@suda.edu.cn (Z. Zhong).

http://dx.doi.org/10.1016/j.jconrel.2016.05.014
0168-3659/

cells [29]. In addition, redox-responsive PCL-SS-PEEP nanoparticles could overcome multidrug resistance due to rapid drug release in MDR cells [30]. These *in vitro* results demonstrate that reduction-sensitive shell-sheddable biodegradable micelles are promising systems for anticancer drug delivery. The fast triggered intracellular drug release is due to the presence of a high glutathione level in the cytoplasm of tumor cells [31–37]. It is interesting to note, nevertheless, that though *in vitro* results are highly promising, reduction-sensitive shell-sheddable biodegradable micelles have not been studied *in vivo*. It has been reported that disulfide-containing delivery systems might encounter stability issues in the circulation due to thiol-disulfide exchange reactions caused by the thiol pools (*e.g.*, Cys/CySS pool) in the blood circulatory system [38]. Taking the most advanced antibody drug conjugates (ADCs) as an example, trastuzumab DM1 conjugates with disulfide linker (SPDP) were pharmacokinetically less stable as compared to FDA approved non-reducible trastuzumab-MCC-DM1 (Kadcyla®) [39], implying the necessity to investigate the stability of disulfide-containing delivery system in the blood circulation.

In this paper, we report on the *in vivo* pharmacokinetics, biodistribution, and therapeutic effects of DOX-loaded cRGD-functionalized reduction-sensitive shell-sheddable biodegradable PEG-SS-PCL micelles in U87MG glioma xenografts (Scheme 1). Here, we selected cRGD peptide as a model targeting ligand because it shows a high affinity for $\alpha_v\beta_3$ integrins, which are important biomarkers overexpressed on angiogenic tumor endothelial cells as well as varying malignant tumor cells such as U87MG glioblastoma cells and B16 melanoma cells [40–44].

2. Materials and methods

2.1. Materials

Poly(ethylene glycol) monomethyl ether (MeO-PEG, M_n = 5.0 kg/mol, Fluka, USA) was dried by azeotropic distillation from toluene. ε-Caprolactone (ε-CL, 99%, Alfa Aesar, USA), dichloromethane (DCM, Sinopharm Chemical Reagent Co., Ltd., Shanghai, China) and dimethyl sulfoxide (DMSO, Sinopharm Chemical Reagent Co., Ltd., Shanghai, China) were dried by refluxing over CaH_2 and distilled before use. 1-(3-Dimethylaminopropyl)-3-ethylcarbodiimide hydrochloride (EDC·HCl, 98%, J&K, Beijing, China), *N*-hydroxysuccinimide (NHS, 98%, Alfa Aesar, USA), triethylamine (99%, Alfa Aesar, USA), mercaptopropionic acid (99%, J&K, Beijing, China), 2,2′-Azobisisobutyronitrile (AIBN, 98%, J&K, Beijing, China), pyrene (>99%, Sigma-Aldrich, USA), triton X-100, hydrochloric acid, isopropanol, diethylether, *N*,*N*-dimethylformamide (DMF), pyridine, paraformaldehyde were all obtained from Sinopharm Chemical Reagent Co., Ltd., Shanghai, China, doxorubicin hydrochloride (>99%, Beijing ZhongShuo Pharmaceutical Technology Development Co., Ltd., Beijing, China), cRGDfK, Cyclo (-Arg-Gly-Asp-D-Phe-Lys), (cRGD, 98%, ChinaPeptides Co., Ltd., Shanghai, China), glutathione (GSH, >98%, Amresco, USA), 2-mercaptopyridine (Py-SH, 99%, Sigma, USA), dithiothreitol (DTT, 99%, Merck, Darmstadt, Germany), p-nitrophenyl chloroformate (p-NPC, 97%, Alfa Aesar, USA), cystamine dihydrochloride (>98%, Alfa Aesar, USA), 2,2′-dithiodipyridine (Py-SS-Py, 99%, Fluka, USA), zinc bis[bis(trimethylsilyl)amide] (97%, Sigma-Aldrich, USA), and 1,1′-dioctadecyltetramethyl indotricarbocyanine iodide (DiR, 98%, AAT Bioquest Inc., Sunnyvale, CA, USA), 3-(4,5-dimethylthiazol-2-yl)-2,5-diphenyltetrazolium bromide (MTT, Sigma, USA), DAPI (Invitrogen, USA), trypsin (Jinuo Biomedical Technology, Hangzhou, Zhejiang, China), 6, 24 and 96-well plates (Thermo Fisher Scientific, USA) were used as received.

2.2. Cell culture and animal studies

The human glioma U87MG cell line and human breast cancer MCF-7 cell line were purchased from the cell bank of the Chinese Academy of Sciences (Shanghai, China). U87MG and MCF-7 cells were maintained in DMEM medium (HyClone, Logan, Utah, USA) supplemented with 1% (v/v) penicillin and streptomycin (Jinuo Biomedical Technology, Hangzhou, Zhejiang, China), and 10% (v/v) fetal bovine serum (FBS, Gibco, Invitrogen, USA). The cells were cultured as a monolayer in a humidified atmosphere containing 5% CO_2 at 37 °C.

Female Balb/c nude mice of 4–6 weeks age were purchased from Shanghai SLAC laboratory animal Co., Ltd. (Shanghai, China). Mice

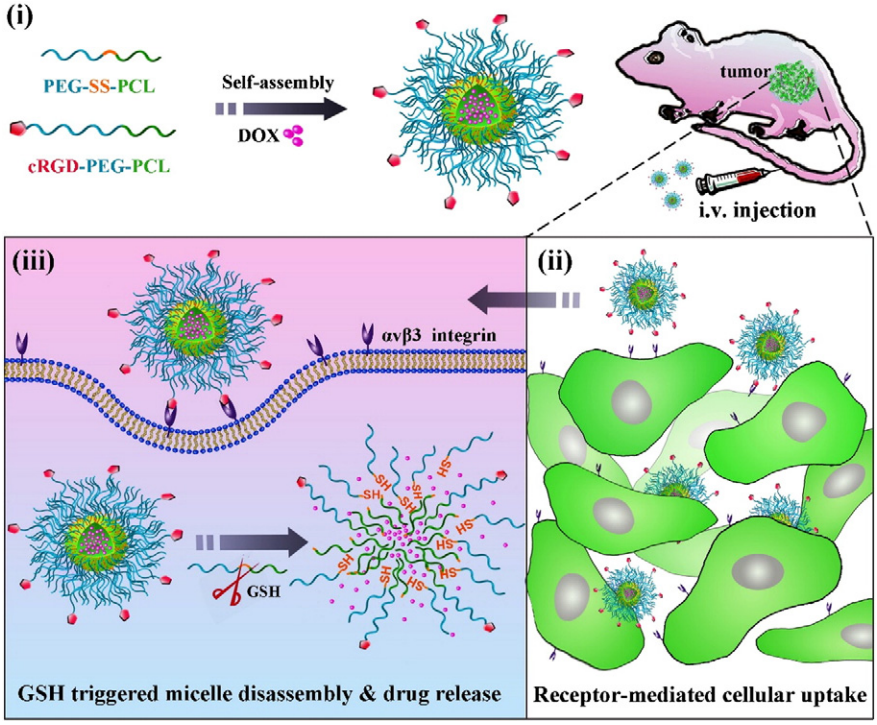

Scheme 1. Illustration of cRGD-functionalized reduction-sensitive shell-sheddable PEG-SS-PCL micelles for targeted and triggered DOX delivery *in vivo*. (i) The micelles are assembled from PEG-SS-PCL and cRGD-PEG-PCL block copolymers; (ii) DOX-loaded micelles actively target to and efficiently accumulate in $\alpha_v\beta_3$-overexpressing U87MG glioma tumor; and (iii) DOX is quickly released into the cytoplasm as a result of GSH-triggered shell shedding.

were housed at 25 °C and 55% humidity under natural light/dark conditions and allowed free access to standard food and water (Shanghai SLAC laboratory animal Co., Ltd., Shanghai, China). All animal procedures were performed following the protocol approved by the Animal Study Committee of Soochow University.

2.3. Synthesis of polymers

cRGD-PEG-PCL was prepared as previously reported with slight modifications [42]. Firstly, under a N_2 atmosphere, allyl-PEG-b-PCL (0.50 g, 46 μmol, 1 eq.), mercaptopropionic acid (0.01 g, 0.93 mmol, 20 eq.) and AIBN (0.11 g, 0.69 mmol, 15 eq.) were added to dry DMF (6 mL). The mixture was stirred at 70 °C for 24 h. The adduct, HOOC-PEG-b-PCL, was isolated by precipitation in cold diethyl ether, washed several times with diethyl ether, and dried *in vacuo* at room temperature. Yield: 86.3%. HOOC-PEG-b-PCL (0.2 g, 18 μmol, 1 eq.) was reacted with cRGD (21.7 mg, 36 μmol, 2 eq.) in 3 mL of DMF in the presence of EDC (10.6 mg, 56 μmol, 3 eq.) and NHS (3.2 mg, 28 μmol, 1.5 eq.). The reaction was carried out for 24 h at room temperature. The final product, cRGD-PEG-PCL, was isolated through dialysis against deionized water for 48 h (MWCO 7000 Da) followed by lyophilization. Yield: 95.4%. ^{1}H NMR (400 MHz, DMSO-d_6): PEG: δ 3.51; PCL: δ 1.30, 1.54, 2.30, 3.99; cRGD moiety: δ 6.62, 6.90 (Fig. S4). M_n (GPC) = 17.6 kg/mol. The degree of cRGD conjugation was determined to be 96% by the Micro BCA Protein assay kit (Pierce, Thermo Scientific, USA).

PEG-PCL diblock copolymer, was synthesized by ring-opening polymerization of ε-CL in DCM at 40 °C using MeO-PEG as an initiator and zinc bis[bis(trimethylsilyl)amide] as a catalyst. Briefly, in a glove-box under a nitrogen atmosphere, zinc bis[bis(trimethylsilyl)amide] (19 mg, 50 μmol, 0.5 eq.) was quickly added to a stirred solution of PEG (0.50 g, 100 μmol, 1 eq.), ε-CL (0.30 g, 2.63 mmol, 2.6 eq.) in DCM (4.0 mL). The reaction vessel was sealed and placed into an oil-bath thermostated at 40 °C. The polymerization was allowed to proceed with magnetic stirring for 48 h. The resulting polymer was isolated by precipitation in cold diethylether, filtration, and drying *in vacuo*. M_n (^{1}H NMR) = 8.1 kg/mol, M_n (GPC) = 16.1 kg/mol, PDI (GPC) = 1.21.

PEG-SS-PCL (M_n = 5.0–3.1 kg/mol, PDI = 1.12, Fig. S1 and S2) and allyl-PEG-b-PCL (M_n = 6.4–3.2 kg/mol, PDI = 1.09, Fig. S3) were synthesized according to our previous reports [12,45].

2.4. Characterization of polymers

^{1}H NMR spectra were recorded on a Unity Inova 400 spectrometer (Agilent, USA) operating at 400 MHz using deuterated chloroform ($CDCl_3$, CIL, Andover, MA, USA) or deuterated dimethylsulfoxide (DMSO-d_6, CIL, Andover, MA, USA) as a solvent. The molecular weight and polydispersity of the copolymers were determined using a gel permeation chromatograph (GPC) instrument (Waters 1515, USA) equipped with two linear PL gel columns (500 Å and Mixed-C) following a guard column and a differential refractive-index detector (RI 2414). The measurements were performed using DMF as the eluent at a flow rate of 1.0 mL/min at 30 °C and a series of narrow polystyrene standards for the calibration of the columns.

2.5. Preparation and characterization of blank and DOX-loaded micelles

Typically, cRGD functionalized reduction-sensitive micelles with different densities of cRGD were prepared by direct injection of 100 μL of cRGD-PEG-PCL and PEG-SS-PCL block copolymers at a predetermined molar ratio (10/90, 20/80 and 30/70) in DMF (10 mg/mL) into 0.9 mL of phosphate buffer (PB, 10 mM, pH 7.4) and standing at room temperature for 2 h to form a homogeneous dispersion, followed by extensive dialysis against PB for 12 h at room temperature. The cRGD functionalized reduction-insensitive cRGD/PEG-PCL micelles and non-targeting reduction-sensitive PEG-SS-PCL micelles were used as control groups and prepared in a similar way.

The critical micelle concentration (CMC) was determined using pyrene as a fluorescence probe.

Hydrophobic DOX was obtained by adding 2.4 mL of triethylamine (Et_3N) to DOX·HCl solution (5 mg DOX·HCl dissolved in 0.98 mL DMSO) followed by stirring overnight at 37 °C in the dark, removing the supernatant containing excess Et_3N and Et_3N·HCl, and finally stirring overnight to remove residual Et_3N by vaporization. Preparation of DOX-loaded micelles was similar to that of blank micelles except that the organic phase was a mixture of block copolymers (5 mg/mL in DMF) and hydrophobic DOX (5 mg/mL in DMSO). To determine the drug loading content (DLC) and drug loading efficiency (DLE), DOX-loaded micelle suspensions were freeze-dried, dissolved in DMF and analyzed with fluorescence spectroscopy (Agilent Technologies, USA) at Ex = 480 nm, Em = 560 nm. A calibration curve was obtained with DOX/DMF solutions with different DOX concentrations. DLC and DLE were calculated according to the following formulae:

$$\text{DLC (wt\%)} = (\text{weight of loaded drug/total weight of polymer and loaded drug}) \times 100$$
$$\text{DLE (wt\%)} = \text{weight of loaded drug/weight of drug in feed} \times 100$$

The size of micelles was determined using dynamic light scattering (DLS). Measurements were carried out at 25 °C using a Zetasizer Nano-ZS (Malvern Instruments, UK) equipped with a 633 nm He-Ne laser using back-scattering detection. Transmission electron microscopy (TEM) was performed using a Tecnai G220 TEM (Hillsboro, OR, USA) operated at an accelerating voltage of 200 kV.

The quenching of DOX in DOX-loaded PEG-SS-PCL micelles was investigated by measuring the fluorescence spectra of PEG-SS-PCL micelles with different DOX loadings (2.5%, 5%, 10%, 20%).

2.6. Serum stability and reduction-triggered destabilization of micelles

The stability of PEG-SS-PCL and cRGD20/PEG-SS-PCL micelles in the presence of 10% FBS was assessed by DLS. Samples were maintained at 37 °C in a shaking bath (THZ-C, Taicang Instrument Factory, Jiangsu, China) at 200 rpm, for 24 h. At desired time intervals, the sizes were determined by DLS.

The destabilization of cRGD20/PEG-SS-PCL micelles in response to 10 mM or 20 μM GSH in PB buffer (10 mM, pH 7.4) was investigated by DLS measurements. Briefly, cRGD20/PEG-SS-PCL micelle dispersion and GSH solution (the pH was adjusted to 7.4 with 1 M NaOH) were gently bubbled with nitrogen gas for 10 min, respectively. Then GSH solution was quickly added into the micelle dispersion (final GSH concentration: 10 mM or 20 μM) and the mixture was immediately placed in a shaking bath (200 rpm) at 37 °C. At different time intervals, the micelle size was measured using DLS. PEG-SS-PCL and cRGD20/PEG-PCL micelles were used as control groups.

2.7. Reduction-triggered drug release

The *in vitro* release of DOX from micelles was studied using a dialysis tube (Spectra/Pore, MWCO 12000) at 37 °C in PB (10 mM, pH 7.4) either in the presence or absence of 10 mM or 20 μM GSH. To acquire sink conditions, drug release studies were performed at a micelle concentration of 1.0 mg/mL (DOX concentration ~175 μg/mL) with 0.5 mL of micelle dispersion dialyzed against 25 mL of the same media. At desired time intervals, 5 mL of release medium was taken out and replenished with an equal volume of fresh medium. The amount of DOX released was determined by using fluorescence measurements.

2.8. Cellular uptake of micelles

Cellular uptake of micelles was analyzed by confocal laser scanning microscopy (CLSM, Leica TCS SP5, Wetzlar, Germany) and flow cytometry (FACS Calibur, BD Biosciences, USA). For confocal studies, U87MG cells were seeded on round glass coverslips at a density of 2×10^4 cells/well

in 24-well plates and cultured at 37 °C for 24 h. DOX-loaded micelles were added and incubated for 4 h or 12 h at a DOX concentration of 10 μg/mL. The culture medium was removed and the cells were washed with PBS. The cell nuclei were stained with DAPI for 10 min. The cells following three times washing with PBS, fixation using 4% (w/v) paraformaldehyde, and three times washing again with PBS were examined with CLSM.

For flow cytometry analysis, U87MG cells were seeded at a density of 2×10^5 cells/well in 6-well plates and cultured for 24 h. DOX-loaded micelles were added and incubated for 4 h at a DOX concentration of 10 μg/mL. The cells were washed three times with PBS, detached with trypsin, centrifuged at 156.5 ×*g* for 5 min and suspended in 0.5 mL of PBS. The cells were analyzed using flow cytometry at the FL2-channel (excitation 488 nm and emission ~575 nm). For each sample, 10,000 events were collected and U87MG cells cultured under normal conditions were used as the control.

2.9. MTT assay

The antitumor activity of DOX-loaded micelles and free DOX·HCl were determined by the MTT assay. Briefly, U87MG cells were seeded at a density of 8×10^3 cells/well in 96-well plates and cultured for 12 h. The prescribed amounts of DOX-loaded micelles or free DOX·HCl in 10 μL of PBS were added. The cells were incubated for 4 h, the medium was removed and replaced with fresh medium, and the cells were incubated for another 44 h. Subsequently, 20 μL of MTT stock solution (5 mg/mL) was added to each well, and the plates were further incubated for 4 h at 37 °C in the dark. The medium was discarded and 100 μL of DMSO was added to dissolve the blue formazan crystals. Cell viability was assessed by the absorbance at 492 nm of the DMSO solution measured on a microplate reader. The data were expressed as the percentages of viable cells compared to the survival of a control group (untreated cells).

2.10. In vivo pharmacokinetics

The mice were handled under protocols approved by Soochow University Laboratory Animal Center and the Animal Care and Use Committee of Soochow University. The DOX level in blood was measured by drawing ~10 μL of blood from the tail vein of nude mice at different time points post-injection of DOX loaded PEG-SS-PCL, cRGD20/PEG-PCL, cRGD20/PEG-SS-PCL or free DOX·HCl (10 mg DOX equiv./kg). Each blood sample was dissolved in 0.15 mL of lysis buffer (1% v/v Triton X-100) with brief sonication. DOX was extracted by incubating blood samples in hydrochloric acid-isopropanol (HCl-IPA) at −20 °C overnight. The samples were vortexed and centrifuged at 30,065 ×*g* for 15 min. The DOX level of the supernatant was determined by fluorescence measurement. Data are presented as the percentage injected dose per gram blood (%ID/g). The elimination half-life ($t_{1/2\beta}$) was calculated by fitting the experimental data using Software Origin8 exponential decay 2 model: $y = A_1 \times \exp(-x/t_1) + A_2 \times \exp(-x/t_2) + y_0$, and taking $t_{1/2\beta} = 0.693 \times t_2$.

2.11. In vivo imaging

Tumor-bearing mice were established as described previously [42]. Briefly, about 1×10^7 U87MG cells were subcutaneously injected in the scapular region of the mice. Tumors were allowed to grow to an average volume of about 50 mm^3 in diameter before the experiment. The fluorescent dye DiR was entrapped into the micelles to investigate the tumor targeting efficacy of different types of micelles *in vivo*. In a typical example, PEG-SS-PCL (4 mg, 0.5 μmol), cRGD-PEG-PCL (1.25 mg, 0.125 μmol) and DiR (0.05 mg, 1% drug loading content) were dissolved in 200 μL DMF, mixed thoroughly and then injected into 1.0 mL of PB (10 mM, pH 7.4). The solution was kept at room temperature for 2 h and then extensively dialyzed against PB buffer for 12 h at room temperature. The quenching of DiR in DiR-loaded PEG-SS-PCL micelles with different DiR loadings (0.5%, 1%, 2.5%, 5%) was investigated in a similar way as for DOX-loaded micelles described above. DiR-loaded PEG-SS-PCL, cRGD20/PEG-PCL or cRGD20/PEG-SS-PCL micelles were injected into tumor-bearing mice *via* the tail vein at a DiR concentration of 25 μg/mL, respectively. At 4, 8, 12, 24 and 72 h post injection, the mice were anesthetized, and whole body fluorescence images were acquired using a near-infrared fluorescence imaging system (Kodak, Rochester, New York) with a wavelength set at Ex = 748 nm, Em = 780 nm. During the imaging acquiring process, 3% isoflurane anesthesia (Abbott laboratories, Chicago, IL) was delivered to the mice *via* a nose cone system. The fluorescence intensity of DiR at the tumor site was measured by using the region of interest (ROI) function and data are presented as means ± SD (n = 3).

2.12. Biodistribution

To quantify the amount of DOX delivered to the tumor and different organs, U87MG tumor-bearing mice following 4 h i.v. injection with DOX loaded PEG-SS-PCL, cRGD20/PEG-PCL, cRGD20/PEG-SS-PCL micelles or free DOX·HCl (10 mg DOX equiv./kg) were sacrificed. The tumor and organs including heart, liver, spleen, lung, and kidney were collected, washed with cold saline, weighed, and homogenized in 0.6 mL of 1% Triton X-100. Then 0.9 mL of the extraction solution (HCl-IPA) was added, and the samples were incubated at −20 °C overnight. After vortexing and centrifugation at 17, 226 ×*g* for 15 min, the DOX level of the supernatant was determined by fluorescence measurement. Data are presented as the percentage injected dose per gram tissue (%ID/g). The corresponding tumor-to-normal tissue (T/N) distribution ratios were calculated according to the formulae: T/N(%) = (percentage injected dose per gram tumor/percentage injected dose per gram normal tissue) × 100.

2.13. In vivo antitumor efficacy

Nude mice bearing U87MG glioma xenografts were used to evaluate the efficacy of DOX-loaded PEG-SS-PCL, cRGD20/PEG-PCL, cRGD20/PEG-SS-PCL micelles and free DOX·HCl. The treatments were initiated when the tumor reached a volume of 30–40 mm^3. The day starting the treatment was designated as day 0. On day 0, the mice were randomly divided into six groups of 5 mice and injected intravenously *via* the tail vein with the above formulations (10 mg DOX equiv./kg). The treatment was repeated every 4 days for a total of 7 doses. The injection volume was 0.2 mL per 20 g of mouse body weight. The tumor sizes were measured by calipers and the volume was calculated according to the formula $V = 0.5 \times L \times W \times H$, wherein L is the tumor dimension at the longest point, W is the tumor dimension at the widest point and H is the height of the tumor.

2.14. Statistical analysis

All data are presented as the mean ± standard deviation (SD). One-way analysis of variance (ANOVA) was used to determine significance among groups, after which post-hoc tests with the Bonferroni correction were used for comparison between individual groups. Statistical significance was established at $p < 0.05$. * $p < 0.05$, ** $p < 0.01$, *** $p < 0.001$.

3. Results and discussion

3.1. Preparation and triggered drug release behavior of cRGD-functionalized reduction-sensitive shell-sheddable micelles

cRGD-functionalized reduction-sensitive shell-sheddable micelles (cRGD/PEG-SS-PCL) were readily prepared from PEG-SS-PCL (5.0–3.1 kg/mol) and cRGD-PEG-PCL (6.4–3.2 kg/mol) copolymers (Table S1). In order to expose the cRGD ligand at the micelle outer

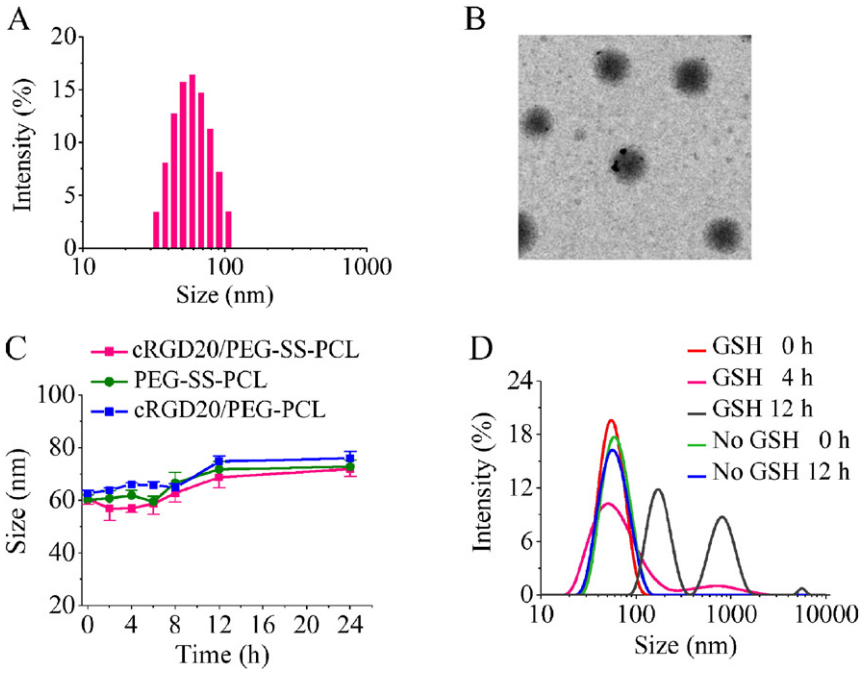

Fig. 1. Size and stability of blank cRGD20/PEG-SS-PCL micelles. The size distribution of cRGD20/PEG-SS-PCL micelles determined by DLS (A) and TEM (B). (C) The serum stability (against 10% FBS, n = 3) of cRGD20/PEG-SS-PCL micelles. cRGD20/PEG-PCL micelles and PEG-SS-PCL micelles were used as controls. (D) GSH-triggered destabilization (against 10 mM GSH) of cRGD20/PEG-SS-PCL micelles.

surface, the PEG in cRGD-PEG-PCL was designed longer than that in PEG-SS-PCL (6.4 *vs* 5.0 kg/mol). It is known that ligand density is an important factor for efficient active tumor-targeting [46,47]. Here, we prepared different densities (10%, 20% and 30%) of cRGD functionalized PEG-SS-PCL micelles by adjusting the molar ratios of cRGD-PEG-PCL to PEG-SS-PCL (corresponding micelles were denoted as cRGD10/PEG-SS-PCL, cRGD20/PEG-SS-PCL and cRGD30/PEG-SS-PCL, respectively). Table S2 displayed that cRGD/PEG-SS-PCL micelles with different cRGD densities had a similar size (61–63 nm), which was comparable to that of PEG-SS-PCL micelles (56 nm). Then we established the optimal cRGD density by flow cytometry. Fig. S5 shows that U87MG cells treated with DOX-loaded cRGD20/PEG-SS-PCL micelles exhibited stronger fluorescence intensity, which was about 3.8-fold and 2.2-fold stronger than those treated with non-targeted PEG-SS-PCL and cRGD10/PEG-SS-PCL counterparts, respectively; supporting that cRGD peptide decoration facilitates the internalization of PEG-SS-PCL micelles into U87MG cells. Notably, increase of cRGD density to 30% did not further increase intracellular DOX fluorescence, indicating that 20% cRGD peptide density is optimal for efficient interaction with surface $\alpha_v\beta_3$ receptors of U87MG cells [40].

Therefore we fixed the density of cRGD to 20% and PEG-SS-PCL micelles and cRGD20-functionalized PEG-PCL micelles (cRGD20/PEG-PCL) were prepared as non-targeting and reduction-insensitive controls, respectively. DLS showed that cRGD20/PEG-SS-PCL micelles had a narrow size distribution and a small size of 61 nm (Fig. 1A). TEM demonstrated that cRGD20/PEG-SS-PCL micelles had a uniform spherical morphology and an average size of about 50 nm (Fig. 1B), which was close to that determined by DLS. Fig. 1C revealed that cRGD20/PEG-SS-PCL micelles as well as PEG-SS-PCL micelles and cRGD20/PEG-PCL micelles were rather stable against 10% FBS likely due to the protection of the PEG layer [48,49]. However, in an intracellular-mimicking reductive environment (10 mM GSH), cRGD20/PEG-SS-PCL micelles disassembled and formed large aggregates (Fig. 1D), similar to PEG-SS-PCL micelles (Fig. S6 A) [12], while there was no size change for reduction-insensitive cRGD20/PEG-PCL micelles (Fig. S6 B). We also investigated the stability of cRGD20/PEG-SS-PCL micelles in the presence of 20 μM GSH which mimics the reducing environment of the circulatory system. No size change was observed after 12 h incubation (Fig. S7 A), indicating that this slightly reducing environment had little effect on our shell-sheddable micelles.

Hydrophobic DOX was loaded into the micelles at a theoretical drug loading content (DLC) of 20.0 wt%. The results showed a drug loading efficiency (DLE) of 74.5% for cRGD20/PEG-SS-PCL micelles, which led to a decent DOX loading of 15.7 wt% (Table 1). Notably, the loading of DOX had little influence on the micellar size. The *in vitro* release studies confirmed that DOX release from cRGD20/PEG-SS-PCL micelles was triggered by 10 mM GSH (Fig. 2). In the presence of 10 mM GSH, 72.3% drug was released from cRGD20/PEG-SS-PCL micelles in 12 h. In contrast, only 14.1% drug was released under a non-reductive condition. It should further be noted

Table 1
Characterization of blank and DOX-loaded cRGD20/PEG-SS-PCL micelles, PEG-SS-PCL micelles, and cRGD20/PEG-PCL micelles (theoretical DLC = 20 wt%).

Sample	Blank micelles		DOX-loaded micelles		DLC (wt%)[a]	DLE (wt%)[a]	CMC (mg/L)[c]
	Size (nm)[b]	PDI[b]	Size (nm)[b]	PDI[b]			
cRGD20/PEG-SS-PCL	61 ± 1.2	0.09	62 ± 3.1	0.16	14.9	70.2	6.8
PEG-SS-PCL	56 ± 0.8	0.12	65 ± 2.1	0.11	15.5	73.3	7.4
cRGD20/PEG-PCL	64 ± 2.6	0.14	66 ± 2.7	0.18	15.7	74.5	6.3

[a] Determined by dynamic light scattering (DLS), n = 3.
[b] Determined by fluorescence measurement, n = 3.
[c] Determined using pyrene as a fluorescent probe, n = 3.

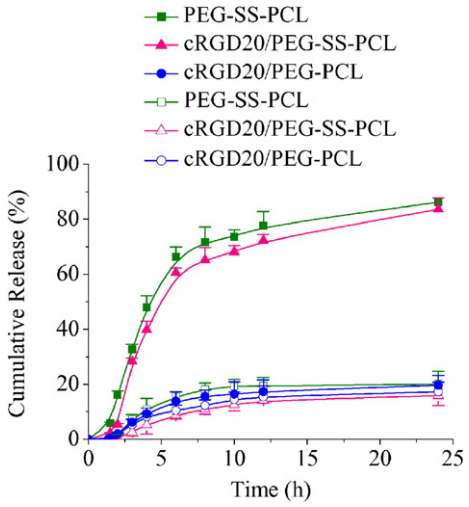

Fig. 2. *In vitro* drug release profiles of DOX-loaded cRGD20/PEG-SS-PCL micelles, either in the presence (filled symbols) or absence (open symbols) of 10 mM GSH, at pH 7.4 and 37 °C. DOX-loaded PEG-SS-PCL micelles and cRGD20/PEG-PCL micelles were used as controls. Data are presented as mean ± SD (n = 3).

that cRGD20/PEG-SS-PCL micelles had almost the same release profiles as PEG-SS-PCL micelles, indicating that the incorporation of 20% cRGD-PEG-PCL into PEG-SS-PCL micelles has no profound effect on the DOX release. In comparison, DOX release from cRGD20/PEG-PCL micelles (reduction-insensitive control) was not enhanced by 10 mM GSH. The drug release of cRGD20/PEG-SS-PCL micelles was also investigated under a blood circulation-mimicking reducing environment (20 μM GSH), which was almost the same as that in the absence of GSH (Fig. S7 B), again demonstrating that cRGD20/PEG-SS-PCL micelles are able to remain intact in this slightly reducing environment.

3.2. In vitro assessment of DOX-loaded cRGD/PEG-SS-PCL micelles

Next, we investigated the cellular uptake behavior of DOX-loaded cRGD20/PEG-PCL, PEG-SS-PCL, cRGD20/PEG-SS-PCL and free DOX·HCl, respectively. As shown in Fig. 3A, although with the same 20% cRGD decoration, cells treated with cRGD20/PEG-PCL micelles for 4 h exhibited much weaker fluorescence intensity than those treated with cRGD20/PEG-SS-PCL micelles, indicating that cRGD20/PEG-SS-PCL micelles mediate faster intracellular DOX release than cRGD20/PEG-PCL micelles. It is known that the fluorescence of DOX is self-quenched if encapsulated in the micelles due to homo Förster resonance energy transfer (homo-FRET) [50–52](Fig. S8). After 12 h incubation, DOX released from cRGD20/PEG-SS-PCL gradually entered into the nucleus, the fluorescence intensity of which was almost comparable with those treated with free DOX·HCl. It was noted that the cytoplasm of cRGD20/PEG-SS-PCL micelles treated cells was still highly fluorescent, probably because it takes much more time for hydrophobic DOX to get across the nuclear membrane while free DOX·HCl rapidly diffuses to the nucleus [53]. Flow cytometry showed that the cellular uptake of DOX for cRGD20/PEG-SS-PCL micelles was about 2.3-fold and 4-fold stronger than that of DOX for PEG-SS-PCL micelles and DOX for cRGD20/PEG-PCL micelles, respectively (Fig. 3B), which is consistent with the CLSM observations. However, in $\alpha_v\beta_3$ negative MCF-7 breast cancer cells, no difference was observed in the cellular uptake of DOX between cRGD20/PEG-SS-PCL micelles and PEG-SS-PCL micelles (Fig. 3C). The above results indicate that cRGD20/PEG-SS-PCL micelles can efficiently target to $\alpha_v\beta_3$ overexpressing U87MG cells and efficiently deliver and release DOX into the nuclei of the cells.

The *in vitro* antitumor efficiency of DOX-loaded micelles was investigated by the MTT assay using U87MG cells. We firstly evaluated the cytotoxicity of blank micelles. The results showed that even at a high micelle concentration (1 mg/mL, corresponding to a system with ~175 μg DOX/mL in DOX-loaded micelles), the cell viability was over 92% (Fig. 4A), corroborating that cRGD20/PEG-SS-PCL micelles are practically non-cytotoxic. Then, the cytotoxicity of DOX-loaded micelles was

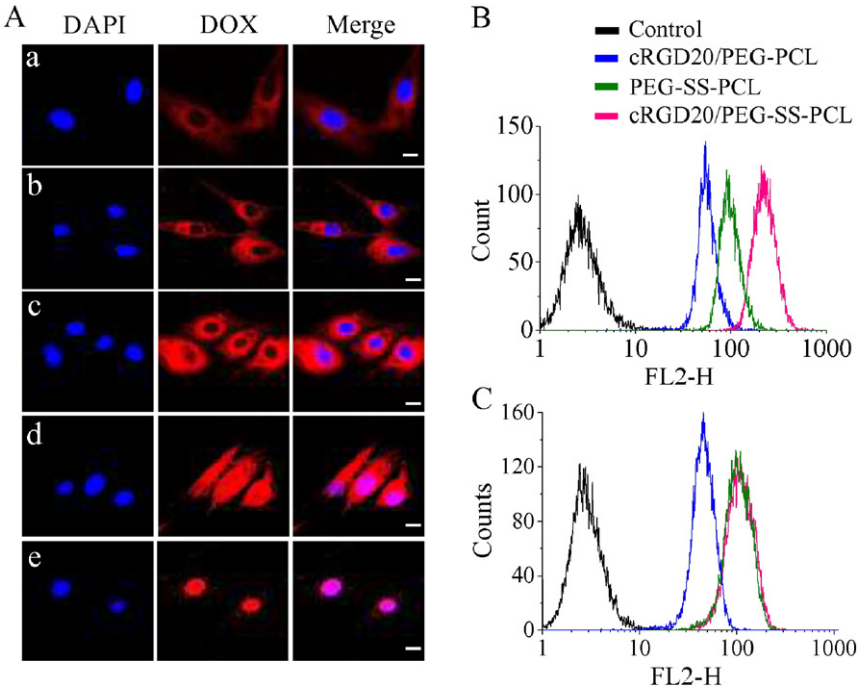

Fig. 3. Cellular uptake and intracellular drug release behavior of DOX-loaded micelles in $\alpha_v\beta_3$ overexpressing U87MG cells. (A) CLSM images of U87MG cells following 4 h incubation with DOX-loaded cRGD20/PEG-PCL micelles (a), 4 h incubation with DOX-loaded PEG-SS-PCL micelles (b), 4 h incubation with DOX-loaded cRGD20/PEG-SS-PCL micelles (c), 12 h incubation with DOX-loaded cRGD20/PEG-SS-PCL micelles (d), and 12 h incubation with free DOX·HCl (e). The scale bars correspond to 10 μm in all the images. Flow cytometry studies of DOX-loaded cRGD20/PEG-SS-PCL micelles compared to DOX-loaded PEG-SS-PCL micelles and DOX-loaded cRGD20/PEG-PCL micelles in $\alpha_v\beta_3$ overexpressing U87MG cells (B) and $\alpha_v\beta_3$ negative MCF-7 cells (C). DOX-loaded micelles were added and incubated for 4 h at a DOX concentration of 10 μg/mL. Cells without any treatment were set as control.

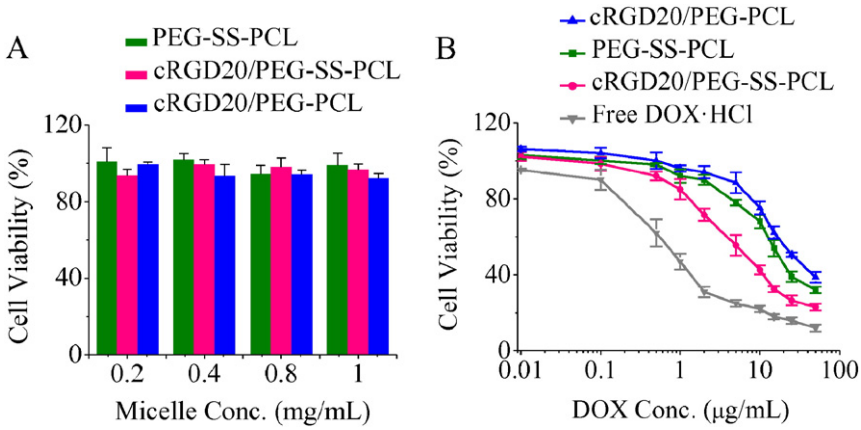

Fig. 4. MTT assays of blank micelles and DOX-loaded micelles in U87MG cells. (A) Viability of U87MG cells following 48 h incubation with blank PEG-SS-PCL, cRGD20/PEG-PCL, and cRGD20/PEG-SS-PCL micelles; and (B) *In vitro* antitumor activity of DOX-loaded cRGD20/PEG-SS-PCL micelles against U87MG cells. The cells were incubated with DOX-loaded cRGD20/PEG-SS-PCL micelles for 4 h, the medium was removed and replenished with fresh culture medium, and the cells were incubated for an additional 44 h. DOX-loaded cRGD20/PEG-PCL micelles, DOX-loaded PEG-SS-PCL micelles and free DOX·HCl were used as controls. Data are presented as mean ± SD (n = 4).

investigated at various DOX concentrations (0.01–50 μg/mL). Fig. 4B showed that cRGD20/PEG-SS-PCL micelles exhibited a high antitumor effect, with a half-maximal inhibitory concentration (IC_{50}) of 6.36 μg/mL, which was 5.3-fold and 2.9-fold lower than that of cRGD20/PEG-PCL (33.75 μg/mL) and PEG-SS-PCL (18.35 μg/mL) controls, respectively. These results further confirm that both active-targeting and reduction-sensitive drug release are critical for PEG-PCL micelles to achieve high antitumor activity.

3.3. In vivo pharmacokinetics and biodistribution in U87MG xenografts

An ideal disulfide-containing drug delivery system (DDS) should remain stable in the blood circulation to avoid premature cleavage [38]. However, some studies showed that thiol-disulfide exchange reactions could also occur in blood, which led to rapid clearance of DDS [39,54]. To investigate the stability of the disulfide bonds in our system, as well as the effect of targeting ligand on circulating time, we tested the half-life time of different DOX-loaded micelles. Fig. 5A displayed that DOX-loaded cRGD20/PEG-SS-PCL micelles had a prolonged elimination half-life time ($t_{1/2\beta}$) of 3.51 h, which was comparable to that for cRGD20/PEG-PCL counterparts, indicating that disulfide bonds in this PEG-SS-PCL micelle system are stable in the circulation. The good stability of cRGD/PEG-SS-PCL micelles in the circulation is likely due to two aspects. One is the relatively weak reductive environment in the blood circulation (approximately 2–20 μM GSH) leading to minimal disulfide exchange reactions [31,38]. The other is the effective steric protection of the disulfide linkages against thiol-containing proteins by the PEG layer [11,38]. As we demonstrated above, the cRGD20/PEG-SS-PCL micelles remained stable and no accelerated drug release was observed in the presence of 20 μM GSH (Fig. S7). In comparison, free DOX·HCl was rapidly eliminated from the circulation with an extremely short $t_{1/2\beta}$ of 0.13 h. It should further be noted that there was no significant difference ($p > 0.05$, ANOVA + post hoc with Bonferroni correction) in $t_{1/2\beta}$ between cRGD20/PEG-SS-PCL micelles and PEG-SS-PCL micelles, indicating that 20% cRGD decoration has little effect on the pharmacokinetics of PEG-SS-PCL micelles.

To visualize the tumor-targeting effect of cRGD20/PEG-SS-PCL micelles *in vivo*, micelles were loaded with DiR, a hydrophobic near infrared fluorescent dye. The U87MG bearing nude mice following tail vein injection of DiR-loaded cRGD/PEG-SS-PCL micelles were imaged using a near-infrared fluorescence imaging system. The results showed that strong DiR fluorescence was observed at the tumor 8 h after injection of DiR-loaded cRGD20/PEG-SS-PCL micelles (Fig. 5Bc). In comparison, mice following 8 h injection with DiR-loaded cRGD20/PEG-PCL (Fig. 5Bb) and PEG-SS-PCL (Fig. 5Ba) micelles displayed much weaker DiR fluorescence and strong DiR fluorescence was observed only at 24 h post injection. It is also interesting to note that the fluorescence intensity in the tumor was maintained for a much longer time for DiR-loaded cRGD20/PEG-SS-PCL micelles than DiR-loaded cRGD20/PEG-PCL and PEG-SS-PCL controls. The strong DiR fluorescence observed for cRGD20/PEG-SS-PCL micelles as compared to cRGD20/PEG-PCL

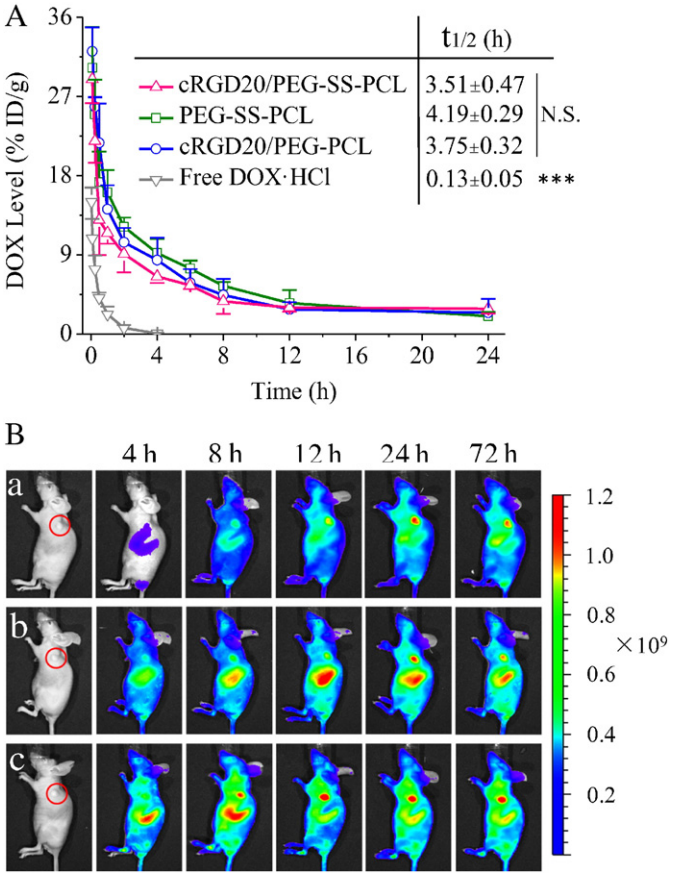

Fig. 5. (A) *In vivo* pharmacokinetics of DOX-loaded cRGD20/PEG-SS-PCL micelles in nude mice (DOX dosage = 10 mg/kg). DOX-loaded PEG-SS-PCL, DOX-loaded cRGD20/PEG-PCL, and free DOX·HCl were used as controls. Data are presented as mean ± SD, n = 3. N.S.: no significance, *** $p < 0.001$, compared with the other three micelle groups. (B) Whole-body images of U87MG tumor-bearing nude mice at various time points after tail vein injection of DiR-loaded PEG-SS-PCL micelles (a), DiR-loaded cRGD20/PEG-PCL micelles (b), or DiR-loaded cRGD20/PEG-SS-PCL micelles (c). The red circle indicates the position of the tumor.

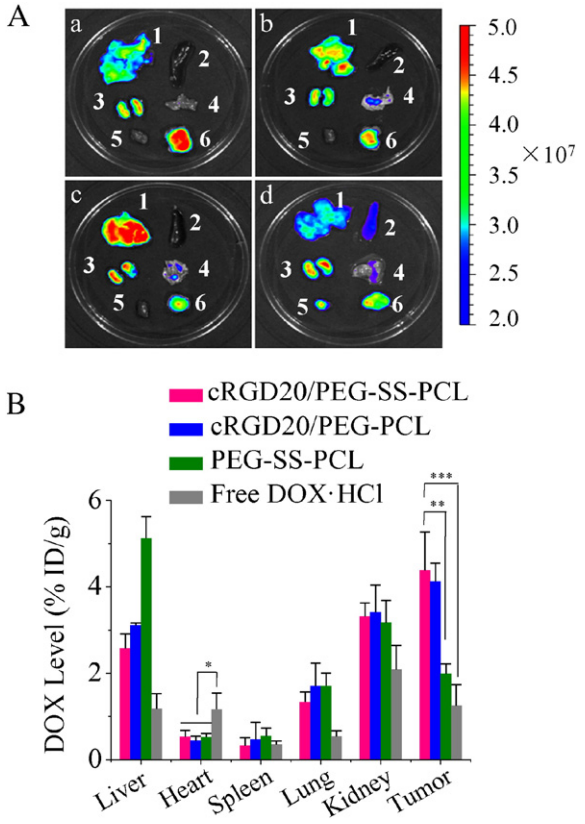

Fig. 6. *In vivo* biodistribution of DOX-loaded cRGD20/PEG-SS-PCL micelles in U87MG tumor-bearing nude mice (DOX dosage = 10 mg/kg) at 4 h post injection. DOX-loaded PEG-SS-PCL, DOX-loaded cRGD20/PEG-PCL, and free DOX·HCl were used as controls. (A) *Ex vivo* DOX fluorescence images of tumors and different organs (1: liver, 2: spleen, 3: kidney, 4: lung, 5: heart and 6: tumor). DOX-loaded cRGD20/PEG-SS-PCL (a), DOX-loaded cRGD20/PEG-PCL (b), DOX-loaded PEG-SS-PCL (c), and free DOX·HCl (d); (B) DOX level, expressed as injected dose per gram of tissue (%ID/g), in the tumor and different organs. * $p < 0.05$, ** $p < 0.01$, *** $p < 0.001$. Data are presented as mean ± SD ($n = 3$).

micelles is likely due to the more efficient release of DiR. As we demonstrated in Fig. S8, DiR is quenched if loaded in a high concentration in the micellar core [55]. When DiR releases from micelles, it will anchor in the cell membrane stably and emits stronger fluorescence [56]. Although the release behavior of DiR-loaded PEG-SS-PCL micelles should be similar as that of DiR-loaded cRGD20/PEG-SS-PCL micelles after arrival in the cytoplasm of the tumor cells, cRGD20/PEG-SS-PCL micelles are actively targeting U87MG tumor cells, leading to an enhanced accumulation of micelles in tumor tissue and subsequent higher amounts of released DiR. The quantitative analysis (Fig. S9) also showed that the fluorescence intensity at the tumor site for DiR-loaded micelles rapidly increased for the first 24 h and then remained almost stable up to 72 h. Obviously, cRGD20/PEG-SS-PCL micelles at the tumor site at 72 h exhibited much stronger fluorescence intensity than the other two groups ($p < 0.01$). The above results confirm that cRGD20/PEG-SS-PCL micelles efficiently deliver and release DiR into U87MG xenografts in mice.

The *in vivo* biodistribution of DOX-loaded cRGD/PEG-SS-PCL micelles was investigated using U87MG tumor-bearing nude mice. The mice were injected *via* the tail vein with DOX-loaded cRGD/PEG-SS-PCL micelles at a DOX dosage of 10 mg/kg. Fig. 6A shows the *ex vivo* DOX fluorescence images of tumor and major organs such as liver, heart, spleen, lung, and kidney isolated from of U87MG bearing mice 4 h post injection. Notably, mice treated with DOX-loaded cRGD20/PEG-SS-PCL micelles exhibited much stronger DOX fluorescence at the tumor than in the other organs, supporting that cRGD20/PEG-SS-PCL micelles have good tumor selectivity and can efficiently release DOX into the tumor. The fluorescence of DOX is self-quenched if not released from the micelles. It should further be noted that the tumor of mice treated with DOX-loaded cRGD20/PEG-SS-PCL micelles exhibited much stronger fluorescence than that with DOX-loaded PEG-SS-PCL, DOX-loaded cRGD20/PEG-PCL, and free DOX·HCl. The quantification of DOX in the tumor and major organs showed that tumor accumulation of DOX was 4.38%ID/g for cRGD20/PEG-SS-PCL micelles, which was the highest among all the organs and was *ca.* 2.2-fold higher than that for PEG-SS-PCL (1.99%ID/g) (Fig. 6B), corroborating that cRGD functionalization facilitates active targeting to U87MG tumor [35,57,58]. Notably, the accumulation in the liver of DOX-loaded cRGD20/PEG-SS-PCL micelles and cRGD20/PEG-PCL micelles as determined by extraction of the organs was lower than that of PEG-SS-PCL micelles (Fig. 6B), probably because of active targeting of cRGD micelles to tumor tissue [42]. It should further be noted that cRGD20/PEG-PCL micelles had a very similar biodistribution profile and tumor accumulation (4.12%ID/g) as cRGD20/PEG-SS-PCL micelles. The DOX fluorescence at the tumor was, however, much weaker for the DOX-loaded cRGD20/PEG-PCL micelles (Fig. 6A), which is most probably related to slow intracellular DOX release. We also observed that DOX accumulation and fluorescence in the heart was significantly lower ($p < 0.01$) for mice treated with DOX-loaded micelles than with free DOX·HCl, which signifies that these micellar formulations can effectively reduce the cardiac toxicity of free DOX·HCl. It is therefore evident that cRGD20/PEG-SS-PCL micelles lead to efficient accumulation in U87MG tumor as well as selective and fast drug release into U87MG tumor cells. The corresponding tumor-to-normal tissue (T/N) distribution ratios of DOX (Table 2) further demonstrate that cRGD20/PEG-SS-PCL micelles have greatly enhanced the DOX accumulation in U87MG tumors while reducing DOX uptake by healthy organs.

3.4. In vivo antitumor efficacy

The *in vivo* antitumor efficacy of DOX-loaded cRGD20/PEG-SS-PCL micelles was studied using U87MG glioma-bearing nude mice and compared to DOX-loaded cRGD20/PEG-PCL, DOX-loaded PEG-SS-PCL, and free DOX·HCl. The mice were injected *via* the tail vein at a drug dosage of 10 mg DOX equiv./kg every 4 days. The results showed that DOX-loaded cRGD20/PEG-SS-PCL micelles caused significantly more effective suppression of tumor growth ($p < 0.05$) than both DOX-loaded PEG-SS-PCL and DOX-loaded cRGD20/PEG-PCL micelles (Fig. 7A), indicating that homing to U87MG tumor cells by cRGD peptide and rapid intracellular drug release both play an important role in effective tumor therapy. Notably, DOX-loaded PEG-SS-PCL and DOX-loaded cRGD20/PEG-PCL micelles could also inhibit tumor growth to a certain extent and exhibited similar antitumor effect as a result of interplay between active tumor targeting and intracellular drug release. PEG-SS-PCL micelles although showing a triggered intracellular drug release behavior cannot be effectively taken up by U87MG tumor cells while cRGD20/PEG-PCL

Table 2
Tumor-to-normal tissue (T/N) distribution ratios of DOX at 4 h post i.v. injection of different DOX-loaded micelles or free DOX·HCl. Data are presented as mean ± SD ($n = 3$).

Formulations	Liver	Heart	Spleen	Lung	Kidney
cRGD20/PEG-SS-PCL	1.71 ± 0.10	8.22 ± 0.49	13.56 ± 3.55	3.29 ± 0.07	1.32 ± 0.08
cRGD20/PEG-PCL	1.32 ± 0.11	9.32 ± 2.13	8.86 ± 4.11	2.42 ± 0.05	1.21 ± 0.02
PEG-SS-PCL	0.39 ± 0.05	3.81 ± 1.82	3.62 ± 1.23	1.16 ± 0.15	0.63 ± 0.05
DOX·HCl	1.05 ± 0.11	1.06 ± 0.08	3.50 ± 1.43	2.28 ± 0.08	0.59 ± 0.09

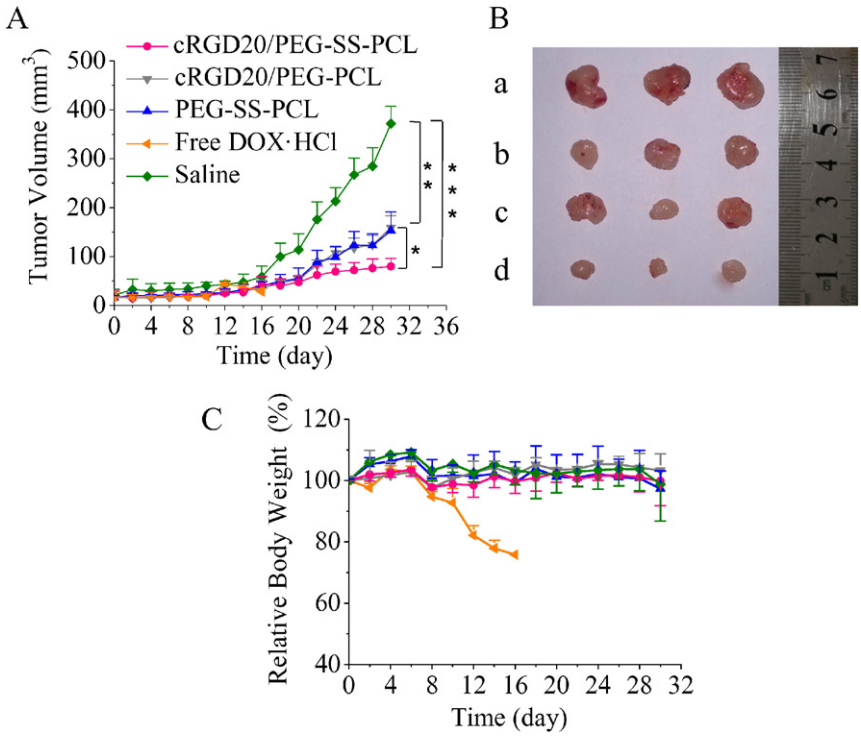

Fig. 7. *In vivo* antitumor performance of DOX-loaded cRGD20/PEG-SS-PCL micelles in U87MG tumor-bearing nude mice. DOX-loaded cRGD20/PEG-PCL micelles, DOX-loaded PEG-SS-PCL micelles, and saline were used as controls. The drug was given on day 0, 4, 8, 12, 16, 20 and 24 (drug dosage = 10 mg DOX/kg). (A) Tumor volume changes in time. Data are presented as mean ± SD (n = 5). (B) Photographs of tumor blocks collected from different treatment groups on day 30 (n = 3). a, saline; b, DOX-loaded cRGD20/PEG-PCL; c, DOX-loaded PEG-SS-PCL; d, DOX-loaded cRGD20/PEG-SS-PCL. (C) Body weight changes of nude mice following different treatments within 30 days. Data are presented as means ± SD (n = 5). For the free DOX·HCl-treated group, 3 mice died at day 16. *$p < 0.05$, ** $p < 0.01$, *** $p < 0.001$.

micelles are efficiently internalized into U87MG tumor cells *via* the receptor-mediated endocytosis mechanism but show slow intracellular drug release. The photographs of tumor blocks of mice isolated at day 30 showed that mice treated with DOX-loaded cRGD20/PEG-SS-PCL micelles had the smallest tumor size (Fig. 7B), confirming that cRGD20/PEG-SS-PCL micelles lead to the best tumor growth inhibition. Notably, mice treated with DOX-loaded RGD20/PEG-SS-PCL micelles, similar to those with DOX-loaded cRGD20/PEG-PCL and DOX-loaded PEG-SS-PCL micelles, had little body weight change compared with the saline treated group (Fig. 7C), confirming that micellar drugs have low side effects [4,59,60]. In contrast, mice treated with free DOX·HCl at the same dosage showed dramatic decrease of body weight. These *in vivo* results point out that cRGD20/PEG-SS-PCL micelles are superior to cRGD20/PEG-PCL micelles in U87MG glioma-targeting drug delivery. These reduction-sensitive shell-sheddable biodegradable micelles have proved to be an advanced platform for targeted tumor chemotherapy, which undoubtedly warrants further exploration.

4. Conclusions

We have demonstrated for the first time that cRGD peptide functionalized, reduction-sensitive, shell-sheddable biodegradable micelles (cRGD20/PEG-SS-PCL) exhibited superior antitumor efficacy as compared to traditional biodegradable micelles (cRGD20/PEG-PCL) in $\alpha_v\beta_3$ integrin overexpressing U87MG glioma bearing nude mice *in vivo*. The results show that incorporation of a disulfide bond between PEG and PCL blocks has no detrimental effect in their *in vivo* pharmacokinetics and biodistribution while significantly enhancing their drug release into the U87MG glioma cells. These reduction-sensitive shell-sheddable biodegradable micelles offer unique advantages of easy preparation and more importantly relatively minor modification of structure and properties as compared to common biodegradable micelles, which render them particularly interesting for clinical translation. Notably, by employing different anticancer drugs and homing ligands, we might achieve targeted chemotherapy of various malignancies. These reduction-sensitive shell-sheddable biodegradable micelles have appeared as a simple, versatile and potentially viable platform for translational nanomedicine.

Acknowledgements

This work is financially supported by research grants from the National Natural Science Foundation of China (NSFC 51173126, 51273139, 51403147 and 51473110), the National Science Fund for Distinguished Young Scholars (NSFC 51225302), and a Project Funded by the Priority Academic Program Development of Jiangsu Higher Education Institutions (PAPD).

Appendix A. Supplementary data

Supplementary data to this article can be found online at http://dx.doi.org/10.1016/j.jconrel.2016.05.014.

References

[1] D. Peer, J.M. Karp, S. Hong, O.C. Farokhzad, R. Margalit, R. Langer, Nanocarriers as an emerging platform for cancer therapy, Nat. Nanotechnol. 2 (2007) 751–760.
[2] M.E. Davis, Z. Chen, D.M. Shin, Nanoparticle therapeutics: an emerging treatment modality for cancer, Nat. Rev. Drug Discov. 7 (2008) 771–782.
[3] C. Deng, Y. Jiang, R. Cheng, F. Meng, Z. Zhong, Biodegradable polymeric micelles for targeted and controlled anticancer drug delivery: promises, progress and prospects, Nano Today 7 (2012) 467–480.
[4] H. Cabral, K. Kataoka, Progress of drug-loaded polymeric micelles into clinical studies, J. Control. Release 190 (2014) 465–476.
[5] W. Lin, Introduction: nanoparticles in medicine, Chem. Rev. 115 (2015) 10407–10409.
[6] C. Sheridan, Proof of concept for next-generation nanoparticle drugs in humans, Nat. Biotechnol. 30 (2012) 471–473.

[7] A.Z. Wang, R. Langer, O.C. Farokhzad, Nanoparticle delivery of cancer drugs, Sci. Transl. Med. 63 (2012) 185–198.
[8] J. Gong, M. Chen, Y. Zheng, S. Wang, Y. Wang, Polymeric micelles drug delivery system in oncology, J. Control. Release 159 (2012) 312–323.
[9] M. Talelli, M. Barz, C.J.F. Rijcken, F. Kiessling, W.E. Hennink, T. Lammers, Core-crosslinked polymeric micelles: principles, preparation, biomedical applications and clinical translation, Nano Today 10 (2015) 93–117.
[10] V.J. Venditto, F.C. Szoka Jr., Cancer nanomedicines: so many papers and so few drugs! Adv. Drug Deliv. Rev. 65 (2013) 80–88.
[11] S. Mura, J. Nicolas, P. Couvreur, Stimuli-responsive nanocarriers for drug delivery, Nat. Mater. 12 (2013) 991–1003.
[12] H. Sun, B. Guo, R. Cheng, F. Meng, H. Liu, Z. Zhong, Biodegradable micelles with sheddable poly(ethylene glycol) shells for triggered intracellular release of doxorubicin, Biomaterials 30 (2009) 6358–6366.
[13] L.-Y. Tang, Y.-C. Wang, Y. Li, J.-Z. Du, J. Wang, Shell-detachable micelles based on disulfide-linked block copolymer as potential carrier for intracellular drug delivery, Bioconjug. Chem. 20 (2009) 1095–1099.
[14] H. Sun, B. Guo, X. Li, R. Cheng, F. Meng, H. Liu, Z. Zhong, Shell-sheddable micelles based on dextran-ss-poly(ε-caprolactone) diblock copolymer for efficient intracellular release of doxorubicin, Biomacromolecules 11 (2010) 848–854.
[15] N.R. Ko, J.K. Oh, Glutathione-triggered disassembly of dual disulfide located degradable nanocarriers of polylactide-based block copolymers for rapid drug release, Biomacromolecules 15 (2014) 3180–3189.
[16] H. Li, Y. Cui, J. Liu, S. Bian, J. Liang, Y. Fan, X. Zhang, Reduction breakable cholesteryl pullulan nanoparticles for targeted hepatocellular carcinoma chemotherapy, J. Mater. Chem. B 2 (2014) 3500–3510.
[17] J. Wang, G. Yang, X. Guo, Z. Tang, Z. Zhong, S. Zhou, Redox-responsive polyanhydride micelles for cancer therapy, Biomaterials 35 (2014) 3080–3090.
[18] T.-B. Ren, Y. Feng, Z.-H. Zhang, L. Li, Y.-Y. Li, Shell-sheddable micelles based on star-shaped poly(ε-caprolactone)-SS-poly(ethyl glycol) copolymer for intracellular drug release, Soft Matter 7 (2011) 2329–2331.
[19] Q. Zhang, N.R. Ko, J.K. Oh, Recent advances in stimuli-responsive degradable block copolymer micelles: synthesis and controlled drug delivery applications, Chem. Commun. 48 (2012) 7542–7552.
[20] X.-Q. Li, H.-Y. Wen, H.-Q. Dong, W.-M. Xue, G.M. Pauletti, X.-J. Cai, W.-J. Xia, D. Shi, Y.-Y. Li, Self-assembling nanomicelles of a novel camptothecin prodrug engineered with a redox-responsive release mechanism, Chem. Commun. 47 (2011) 8647–8649.
[21] B. Khorsand Sourkohi, A. Cunningham, Q. Zhang, J.K. Oh, Biodegradable block copolymer micelles with thiol-responsive sheddable coronas, Biomacromolecules 12 (2011) 3819–3825.
[22] H. Wei, J.G. Schellinger, D.S.H. Chu, S.H. Pun, Neuron-targeted copolymers with sheddable shielding blocks synthesized using a reducible, RAFT-ATRP double-head agent, J. Am. Chem. Soc. 134 (2012) 16554–16557.
[23] Z. Xu, D. Wang, S. Xu, X. Liu, X. Zhang, H. Zhang, Preparation of a camptothecin prodrug with glutathione-responsive disulfide linker for anticancer drug delivery, Chem. Asian. J. 9 (2014) 199–205.
[24] J. Ding, J. Chen, D. Li, C. Xiao, J. Zhang, C. He, X. Zhuang, X. Chen, Biocompatible reduction-responsive polypeptide micelles as nanocarriers for enhanced chemotherapy efficacy in vitro, J. Mater. Chem. B 1 (2013) 69–81.
[25] C. Cui, Y.-N. Xue, M. Wu, Y. Zhang, P. Yu, L. Liu, R.-X. Zhuo, S.-W. Huang, Cellular uptake, intracellular trafficking, and antitumor efficacy of doxorubicin-loaded reduction-sensitive micelles, Biomaterials 34 (2013) 3858–3869.
[26] P. Xu, H. Yu, Z. Zhang, Q. Meng, H. Sun, X. Chen, Q. Yin, Y. Li, Hydrogen-bonded and reduction-responsive micelles loading atorvastatin for therapy of breast cancer metastasis, Biomaterials 35 (2014) 7574–7587.
[27] C. Shi, X. Guo, Q. Qu, Z. Tang, Y. Wang, S. Zhou, Actively targeted delivery of anticancer drug to tumor cells by redox-responsive star-shaped micelles, Biomaterials 35 (2014) 8711–8722.
[28] H.-Y. Wen, H.-Q. Dong, W.-j. Xie, Y.-Y. Li, K. Wang, G.M. Pauletti, D.-L. Shi, Rapidly disassembling nanomicelles with disulfide-linked PEG shells for glutathione-mediated intracellular drug delivery, Chem. Commun. 47 (2011) 3550–3552.
[29] Y. Zhong, W. Yang, H. Sun, R. Cheng, F. Meng, C. Deng, Z. Zhong, Ligand-directed reduction-sensitive shell-sheddable biodegradable micelles actively deliver doxorubicin into the nuclei of target cancer cells, Biomacromolecules 14 (2013) 3723–3730.
[30] Y.-C. Wang, F. Wang, T.-M. Sun, J. Wang, Redox-responsive nanoparticles from the single disulfide bond-bridged block copolymer as drug carriers for overcoming multidrug resistance in cancer cells, Bioconjug. Chem. 22 (2011) 1939–1945.
[31] F. Meng, W.E. Hennink, Z. Zhong, Reduction-sensitive polymers and bioconjugates for biomedical applications, Biomaterials 30 (2009) 2180–2198.
[32] M. Huo, J. Yuan, L. Tao, Y. Wei, Redox-responsive polymers for drug delivery: from molecular design to applications, Polym. Chem. 5 (2014) 1519–1528.
[33] R. Cheng, F. Feng, F. Meng, C. Deng, J. Feijen, Z. Zhong, Glutathione-responsive nanovehicles as a promising platform for targeted intracellular drug and gene delivery, J. Control. Release 152 (2011) 2–12.
[34] B. Deng, P. Ma, Y. Xie, Reduction-sensitive polymeric nanocarriers in cancer therapy: a comprehensive review, Nanoscale 7 (2015) 12773–12795.
[35] X. Jiang, X. Sha, H. Xin, L. Chen, X. Gao, X. Wang, K. Law, J. Gu, Y. Chen, Y. Jiang, Self-aggregated pegylated poly (trimethylene carbonate) nanoparticles decorated with c (RGDyK) peptide for targeted paclitaxel delivery to integrin-rich tumors, Biomaterials 32 (2011) 9457–9469.
[36] R. Cheng, F. Meng, C. Deng, Z. Zhong, Bioresponsive polymeric nanotherapeutics for targeted cancer chemotherapy, Nano Today (2015).
[37] H. Sun, F. Meng, R. Cheng, C. Deng, Z. Zhong, Reduction-sensitive degradable micellar nanoparticles as smart and intuitive delivery systems for cancer chemotherapy, Expert Opin. Drug Deliv. 10 (2013) 1109–1122.
[38] L. Brülisauer, M.A. Gauthier, J.-C. Leroux, Disulfide-containing parenteral delivery systems and their redox-biological fate, J. Control. Release 195 (2014) 147–154.
[39] A. Kamath, S. Iyer, Preclinical pharmacokinetic considerations for the development of antibody drug conjugates, Pharm. Res. 32 (2015) 3470–3479.
[40] Y. Miura, T. Takenaka, K. Toh, S. Wu, H. Nishihara, M.R. Kano, Y. Ino, T. Nomoto, Y. Matsumoto, H. Koyama, H. Cabral, N. Nishiyama, K. Kataoka, Cyclic RGD-linked polymeric micelles for targeted delivery of platinum anticancer drugs to glioblastoma through the blood-brain tumor barrier, ACS Nano 7 (2013) 8583–8592.
[41] D. Zhou, G. Zhang, Z. Gan, c(RGDfK) decorated micellar drug delivery system for intravesical instilled chemotherapy of superficial bladder cancer, J. Control. Release 169 (2013) 204–210.
[42] Y. Zhong, C. Wang, R. Cheng, L. Cheng, F. Meng, Z. Liu, Z. Zhong, cRGD-directed, NIR-responsive and robust AuNR/PEG-PCL hybrid nanoparticles for targeted chemotherapy of glioblastoma in vivo, J. Control. Release 195 (2014) 63–71.
[43] S.J. Zhu, L.L. Qian, M.H. Hong, L.H. Zhang, Y.Y. Pei, Y.Y. Jiang, RGD-modified PEG-PAMAM-DOX conjugate: in vitro and in vivo targeting to both tumor neovascular endothelial cells and tumor cells, Adv. Mater. 23 (2011) H84–H89.
[44] N. Nasongkla, X. Shuai, H. Ai, B.D. Weinberg, J. Pink, D.A. Boothman, J. Gao, cRGD-functionalized polymer micelles for targeted doxorubicin delivery, Angew. Chem. Int. Ed. 116 (2004) 6483–6487.
[45] R. Yang, F. Meng, S. Ma, F. Huang, H. Liu, Z. Zhong, Galactose-decorated cross-linked biodegradable poly(ethylene glycol)-b-poly(ε-caprolactone) block copolymer micelles for enhanced hepatoma-targeting delivery of paclitaxel, Biomacromolecules 12 (2011) 3047–3055.
[46] D.R. Elias, A. Poloukhtine, V. Popik, A. Tsourkas, Effect of ligand density, receptor density, and nanoparticle size on cell targeting, Nanomed. Nanotechnol. 9 (2013) 194–201.
[47] Z. Cheng, A. Al Zaki, J.Z. Hui, V.R. Muzykantov, A. Tsourkas, Multifunctional nanoparticles: cost versus benefit of adding targeting and imaging capabilities, Science 338 (2012) 903–910.
[48] J. Logie, S.C. Owen, C.K. McLaughlin, M.S. Shoichet, PEG-graft density controls polymeric nanoparticle micelle stability, Chem. Mater. 26 (2014) 2847–2855.
[49] K.-L. Veiman, K. Künnapuu, T. Lehto, K. Kiisholts, K. Pärn, Ü. Langel, K. Kurrikoff, PEG shielded MMP sensitive CPPs for efficient and tumor specific gene delivery in vivo, J. Control. Release 209 (2015) 238–247.
[50] S.-Y. Lee, S. Kim, J.Y. Tyler, K. Park, J.-X. Cheng, Blood-stable, tumor-adaptable disulfide bonded mPEG-(Cys) 4-PDLLA micelles for chemotherapy, Biomaterials 34 (2013) 552–561.
[51] H.J. Lee, S.E. Kim, I.K. Kwon, C. Park, C. Kim, J. Yang, S.C. Lee, Spatially mineralized self-assembled polymeric nanocarriers with enhanced robustness and controlled drug-releasing property, Chem. Commun. 46 (2010) 377–379.
[52] H. Kobayashi, P.L. Choyke, Target-cancer-cell-specific activatable fluorescence imaging probes: rational design and in vivo applications, Acc. Chem. Res. 44 (2011) 83–90.
[53] H. Su, Y. Liu, D. Wang, C. Wu, C. Xia, Q. Gong, B. Song, H. Ai, Amphiphilic starlike dextran wrapped superparamagnetic iron oxide nanoparticle clsuters as effective magnetic resonance imaging probes, Biomaterials 34 (2013) 1193–1203.
[54] B.A. Kellogg, L. Garrett, Y. Kovtun, K.C. Lai, B. Leece, M. Miller, G. Payne, R. Steeves, K.R. Whiteman, W. Widdison, H. Xie, R. Singh, R.V.J. Chari, J.M. Lambert, R.J. Lutz, Disulfide-linked antibody-maytansinoid conjugates: optimization of in vivo activity by varying the steric hindrance at carbon atoms adjacent to the disulfide linkage, Bioconjug. Chem. 22 (2011) 717–727.
[55] H. Cho, G.L. Indig, J. Weichert, H.-C. Shin, G.S. Kwon, In vivo cancer imaging by poly (ethylene glycol)-b-poly (ε-caprolactone) micelles containing a near-infrared probe, Nanomed. Nanotechnol. 8 (2012) 228–236.
[56] J. Ruan, H. Song, C. Li, C. Bao, H. Fu, K. Wang, J. Ni, D. Cui, DiR-labeled embryonic stem cells for targeted imaging of in vivo gastric cancer cells, Theranostics 2 (2012) 618–628.
[57] C. Zhan, B. Gu, C. Xie, J. Li, Y. Liu, W. Lu, Cyclic RGD conjugated poly(ethylene glycol)-co-poly(lactic acid) micelle enhances paclitaxel anti-glioblastoma effect, J. Control. Release 143 (2010) 136–142.
[58] M.H. Lee, J.Y. Kim, J.H. Han, S. Bhuniya, J.L. Sessler, C. Kang, J.S. Kim, Direct fluorescence monitoring of the delivery and cellular uptake of a cancer-targeted RGD peptide-appended naphthalimide theragnostic prodrug, J. Am. Chem. Soc. 134 (2012) 12668–12674.
[59] T. Lammers, F. Kiessling, W.E. Hennink, G. Storm, Drug targeting to tumors: principles, pitfalls and (pre-) clinical progress, J. Control. Release 161 (2012) 175–187.
[60] A. Rösler, G.W.M. Vandermeulen, H.-A. Klok, Advanced drug delivery devices via self-assembly of amphiphilic block copolymers, Adv. Drug Deliver. Rev. 64 (2012) 270–279.